

# Interfacial phenomena in nanocapacitors with multifunctional oxides

A. V. Kimmel

*CIC nanoGUNE, Tolosa Hiribidea, 76, San Sebastian, 20018, Spain\**

The analysis of the structure, chemical stability, electronic and ferroelectric properties of the interfaces between Pt(001) and PbZrTiO<sub>3</sub>(001) have been performed with *ab initio* methods. We show that the chemical environment plays a critical role in determining the interfacial reconstruction and charge redistribution at the metal/oxide interfaces. We demonstrate that the difference in interfacial bonds formed at the Pt/PZT interfaces with (TiZr)O<sub>2</sub> - and PbO- termination of PZT essentially defines the effectiveness of the screening, and ease of polarisation switching in PZT-based capacitors. The imperfect screening in Pt/PZT<sub>BO<sub>2</sub></sub>/Pt capacitors is caused by strong interfacial bonds formed at the Pt/PZT<sub>BO<sub>2</sub></sub> interface that is accompanied by the suppressed polarisation of PZT film. In contrast, the capacitors with PbO-terminated PZT show a negligible depolarising field, and high polarisation, which is the consequence of weak bonds formed at the Pt/PZT interfaces. The latter also causes a higher switching barrier than that in the former system.

## I. INTRODUCTION

Stable ferroelectric phases in nanometer-thick films are of great interest for ultra-high density and ferroelectric field effect transistors (FeFETs), thus, the properties of ferroelectrics in ultrathin films has been under intense theoretical and experimental investigation [1–10].

Lead zirconate titanate Pb(Zr<sub>1-x</sub>Ti<sub>x</sub>)O<sub>3</sub> (PZT) is one of the most commonly used ferroelectric materials due to its small coercive field, large polarisation, relatively high Curie temperature, and excellent piezoelectric response. PZT is a disordered solid solution ABO<sub>3</sub> perovskite, with Pb atoms occupying the A-site, and Ti and Zr cations randomly arranged among the B-sites. The material exhibits a rich phase diagram with the transition region,  $x=0.42-0.52$ , known as the morphotropic phase boundary (MPB), where it exhibits its highest piezoelectric response [11, 12].

PZT has found a wide range of applications in piezoelectric sensors, actuators, and non-volatile memories, where the interface between the metal electrode and a functional oxide plays an important role in the performance of the device [5–10, 13–15]. For thin PZT films, in particular, the cycling stability, the imprint performance and the leakage current strongly depend on the interfaces between electrode material and ferroelectric film [6, 14–16].

However, the reliable and precise data on the interfacial properties, whether at the structural, or chemical level, is often difficult to obtain from experiment. In the interfacial region the local chemical and electrostatic environment significantly differs from that of parent materials, and the description of the interface in terms of bulk parameters is unjustified.

In this work, we use density functional theory calculations to provide an insight into the properties of PZT(001)/Pt(001) interfaces. We study interfacial reconstruction, the nature of interfacial bonds, and interfacial charge redistribution. We characterise the stability of the ferroelectric phase in Pt/PZT/Pt metal/oxide nano-capacitors with respect to the size and termination of PZT. We show that the chemical bonding

at the interface plays a critical role in determining the effectiveness of the screening, ease of polarisation switching, and stability of ferroelectric state in perovskite-based capacitors.

## II. METHODS

We carried out our first principles calculations with the CASTEP plane-wave code [17] and ultrasoft pseudopotentials [18]. We chose the Wu-Cohen generalised gradient approximation density functional [19] because it is known to reproduce the structural properties of perovskites with high accuracy.

A 500 eV plane-wave cutoff together with 0.025 Å<sup>-1</sup> density of  $k$ -points Monkhorst-Pack mesh have been used for calculations. The convergence of the total energy and forces per atoms were 0.005 eV and 0.05 eV/Å, respectively.

We model MPB composition of PZT with  $x=0.5$  using one of the stable  $P4mm$  phases found by DFT methods [20]. This phase is characterised by the lattice parameters of  $a=5.625$  Å and  $c=4.261$  Å, and exhibits an alternating columnar arrangement of B-site cations along the polar axis (Fig. 1a, b).

We have modelled a PZT(001) slab terminated with PbO, and (TiZr)O<sub>2</sub> atomic layers, further denoted as AO-, and BO<sub>2</sub> as followed to standard definition of perovskite formula ABO<sub>3</sub>, where A-site cations are Pb, while B-site cations are Ti and Zr. Further, we use Pt/PZT<sub>AO</sub> and Pt/PZT<sub>BO<sub>2</sub></sub> notations for the Pt/PZT interfaces with AO and BO<sub>2</sub> terminations of PZT, respectively. Due to symmetry breaking, each simulated capacitor system is characterised by two electrostatically inequivalent interfaces further denoted as  $P^+$  and  $P^-$  (see Fig. 1).

To reveal the effects of the thickness of ferroelectrics in Pt/PZT/Pt capacitor geometry we have varied the thickness of PZT,  $n$ , from 1.5 (0.06 nm) to 7.5 (3.55 nm) unit cells.

We model metal electrodes using Pt slabs with a 3.998 Å fcc lattice parameter. To achieve the convergence of electrostatic potential inside the metal we used ten layers of the metal electrode overall.

To simulate the effect of the mechanical boundary conditions due to the strain imposed by the substrate, the in-plane lattice constant of PZT was fixed to the theoretical equilib-

\* a.kimmel@nanogune.eu

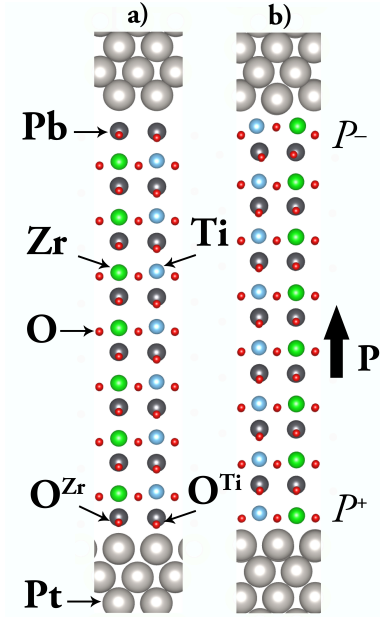


Figure 1. Schematic representation of modelled Pt/PZT capacitor with a) PbO- and b) TiZrO<sub>2</sub> - terminations of PZT. The direction of polar axis is perpendicular to the interface. Due to symmetry breaking there are two inequivalent interfaces further denoted as  $P^+$  and  $P^-$ .

rium lattice constant of bulk Pt, thus, the tensile strain was of 0.6 %. PZT atoms were allowed to relax in all the directions, while only three metal layers in vicinity of the interface were allowed to relax.

The Pt/PZT/Pt nanocapacitors were simulated by using a supercell approximation with imposed periodic boundary conditions. A (1x1) periodicity of the supercell perpendicular to the interface is assumed. This set up gives the electrical short-circuit condition as well as an electrode/perovskite super-lattice geometry. Thus, the formula describing the periodically repeated supercell is Pt<sub>5</sub>/PZT<sub>*n*</sub>/Pt<sub>5</sub>,  $n=1.5, \dots, 7.5$ .

We calculate the rumpling parameter,  $v$ , which provides indirect understanding of a dipole bearing by an atomic layer, as an averaged deviation of cations ( $M$ ) and anions ( $O$ ) in atomic layer,  $i$ , along the polar axis,  $z$  [21]:

$$v_z = \sum_i \delta^z(M_i) - \delta^z(O_i). \quad (1)$$

The band offset at a metal/insulator interface was calculated using a spatially resolved projected density of states (PDOS) by defining the location of the band edges deep in the insulating region, with the Fermi level of the metal taken as a reference [21]:

$$\rho(i, E) = \sum_{nk} \int_B Z < i | \psi_{nk} >|^2 \delta(E - E_{nk}) dk, \quad (3)$$

where  $|i\rangle$  is a normalised function localised in space around the region of interest, and  $\rho(r, E)$  is the local density of states.

The planar-averaged electron charge density normal to the interface was calculated as:

$$\rho(z) = 1/S_{xy} \int \int \rho(x, y, z) dx dy, \quad (4)$$

where  $S_{xy}$  is a cross-section area of the system,  $\rho(x, y, z)$  is three-dimensional charge density and  $\rho(z)$  is its planar averaged derivative.

The planar averaged potential was calculated across the capacitor as:

$$V(z) = 1/S_{xy} \int \int V(x, y, z) dx dy, \quad (5)$$

where  $V(x, y, z)$  is three-dimensional electrostatic potential,  $S_{xy}$  is the cross-section of ferroelectric. The planar averaged potential,  $V(z)$ , exhibits fast oscillations correlated with the atomic arrangement in the material. In order to take the information related to interfaces we have used a macroscopically averaged potential [21]:

$$\langle V(z) \rangle = \int V(z) H(z - z') dz', \quad (6)$$

where  $H(z)$  is the Heaviside step-function taken with the period of the PZT lattice parameter.

### III. RESULTS

#### A. Chemical stability and atomic relaxation

To characterise the interfacial binding energy density  $\sigma$  we calculated the difference between the total energy of the modelling system,  $E_{tot}$ , and the sum of the energy of the PZT slab ( $E_{PZT}$ ) and the Pt slab ( $E_{Pt}$ ) normalised to the surface area,  $S$ , of the interface (since our system has two interfaces we include a factor of 2 into the equation):

$$\sigma = [(E_{PZT}^{slab} + E_{Pt}) - E_{PZT-Pt}]/2S.$$

We have found that both, Pt/PZT<sub>AO</sub> and Pt/PZT<sub>BO<sub>2</sub></sub>, systems are chemically stable. Calculated  $\sigma$  values exhibit a variation with the thickness of PZT. However, the increase of  $n$  leads to a rapid convergence of  $\sigma$  to 0.175 eV/Å<sup>2</sup> and 0.252 eV/Å<sup>2</sup> for Pt/PZT<sub>AO</sub> and Pt/PZT<sub>BO<sub>2</sub></sub> systems, respectively. Thus, it is energetically advantageous to form a Pt/PZT interface, although, the Pt/PZT<sub>BO<sub>2</sub></sub> system is 94.5 meV/Å<sup>2</sup> more stable than Pt/PZT<sub>AO</sub>. The values of the binding energy density are in good agreement with previous *ab initio* calculations of similar Pt/PZT interfaces calculated with open-circuit boundary conditions [6].

We have found a strong difference in the interfacial structure of Pt/PZT related to different chemical environment. The Pt/PZT<sub>AO</sub> interface is characterised by a close contact of the PbO atomic plane with the surface of the metal electrode. One may distinguish different types of oxygen species at the Pt/PZT<sub>AO</sub> interface (See Fig. 1): the oxygen in Pt-O-Zr bonds, further denoted as O<sup>Zr</sup>, and the one in Pt-O-Ti bonds

denoted as  $O^{Ti}$ . We show further that despite the chemical similarity of Ti and Zr cations in PZT [22], the interfacial bonds and the charge transfer at the interface with Pt are different for these species.

With the increase of  $n$ , the length of interfacial Pt- $O^{Ti}$  and Pt- $O^{Zr}$  bonds converges to 2.1 Å and 1.99 Å for  $P^+$ , and to 2.35 Å and 2.7 Å for  $P^-$ , respectively. The electrostatic asymmetry also affects the second neighbours to the interface: for the  $P^-$  interface the short Ti-O and Zr-O bonds are 0.1 Å shorter in comparison to their bulk values (1.91 Å and 1.75 Å for the short Zr-O and Ti-O bonds, respectively), while the long Ti-O and Zr-O bonds at the  $P^+$  interface were elongated by 0.4 Å (2.22 Å and 2.5 Å for long Zr-O and Ti-O bonds, respectively).

Such a difference in bond lengths occurs due the relative proximity of Pb and O ions to the surface of the electrode. The latter affects the electrostatic repulsion between cations dominated by the attraction between O and Pt ions. Such an uncompensated repulsion, as we will later see, leads to the formation of weak Pt-O bonds at the  $P^+$  interface.

The Pt/PZT $_{BO_2}$  interface also shows  $P^-$  and  $P^+$  asymmetry with respect to the interfacial bonds. Indeed, the  $P^+$  interface exhibits relatively short interfacial Pt-O bonds of 2.12 Å. However, the  $P^-$  interface relaxes with two types of Pt-O interfacial bonds: long (2.4 Å) and short (2.12 Å). At the  $P^-$  the B-site cations locate closer to Pt cations than O ions, thus, the repulsion between positive species is partly balanced by the Pt-O attraction.

We have also observed rumpling of the first metal layer of 0.1 Å, which rapidly decays away from the interface.

The analysis of the Crystal Orbital Hamilton Populations curves related to interfacial bonds demonstrates a strong bonding character of interfacial Pt-O bonds at Pt/PZT $_{BO_2}$  interface. Meanwhile, these bonds exhibit a very weak, even non-bonding character at the  $P^-$  side of the Pt/PZT $_{AO}$  interface (See Supplementary Information).

We have found that interfacial bonds formation induces the rotation of oxygen octahedra at the interfacial layers. The rotation of octahedra is characterised with the tilt angle,  $\Theta$  (See Fig. 2). With increasing of PZT thickness a rapid decrease from 8° to 0.5° is observed. We found that the tilt angles of the octahedra based on Zr and Ti cations exhibit different signs, demonstrating an antiferro-distortive nature of the reconstruction at the Pt/PZT interfaces. The tilt angles are bigger at the Pt/PZT $_{AO}$  interface, while the  $P^+$  interface of Pt/PZT $_{BO_2}$  shows negligible angles ( $\Theta < 1^\circ$ ) (See Fig. 2).

A similar phenomenon has been observed at STO/PTO and STO:Nb/PTO interfaces [2]. Here, the rotation of oxygen octahedra was observed in nearly zero-strain systems at open-circuit conditions. The authors have observed a long range octahedral rotation with the critical thickness of 4 nm, above which the rotation disappears.

We assume that the origin of the interfacial rotation of oxygen octahedra at the Pt/ZT/Pt interfaces is related to the minimisation of strain and the depolarising field. While, at the Pt/PZT $_{BO_2}$  interface the octahedral rotation has a lesser amplitude due to the strong interfacial Pt-O bonds formed.

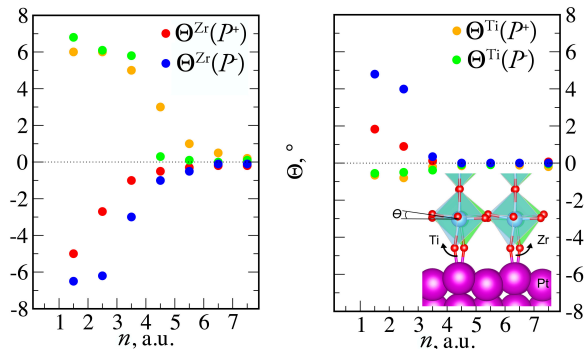


Figure 2. The dependence of the octahedral tilt,  $\Theta$ , on the thickness,  $n$ , at a) Pt/PZT $_{AO}$ , b) Pt/PZT $_{BO_2}$  interfaces.

## B. Rumpling parameter

In the capacitor geometry the formation of the interfacial bonds may affect the polarisation with the possibility of suppression, or enhancement of polarisation in the ferroelectric material [21]. To characterise this, the rumpling parameter,  $v$ , for Pt/PZT $_{AO}$ /Pt and Pt/PZT $_{BO_2}$ /Pt capacitors has been calculated for different thicknesses of PZT (Fig. 3).

Below the critical thickness of  $n_c=4.5$  u.c the rumpling parameter in Pt/PZT $_{AO}$ /Pt exhibits smaller values than that of the bulk PZT (0.49 Å and 0.36 Å for the PbO and TiZrO $_2$  atomic layers, respectively). With  $n > n_c$  the rumpling reaches its bulk limit for the PbO atomic layer, while  $v$  for TiZrO $_2$  layers is 0.2 Å lower than the bulk value. The smallest system ( $n=1.5$  u.c.) exhibits a negative rumpling at the  $P^-$  side. This corresponds to the appearance of a head-to-head domain in PZT (See Fig. 3a).

Notably, the Pt/PZT $_{AO}$ /Pt capacitor shows an enhancement of the rumpling parameter at the  $P^+$  side up to 0.6 Å, because of short Pt-O bonds formed, while the  $P^-$  side exhibits reduced rumpling due to flattening of the interfacial layer.

The overall rumpling parameter in the thin Pt/PZT $_{BO_2}$ /Pt is significantly suppressed and reaches its bulk values for the thicknesses above the critical one,  $n_c$ . The  $P^+$  interface including several adjacent layers is characterised by a reduced rumpling parameter, while, the  $P^-$  interface exhibits its slight increase, which converges to its bulk limit with  $n > 10$ .

We assume that interfacial reconstruction affects Pt/PZT $_{AO}$  interfaces, making PbO atomic layers at  $P^+$  rougher in comparison to bulk PZT. Thus, we expect that polarisation in Pt/PZT $_{AO}$ /Pt will be somehow similar to that in bulk PZT, while in Pt/PZT $_{BO_2}$ /Pt capacitors we expect a suppressed polarisation due to flattening of the atomic layers.

This finding contradicts the conclusion of ref. 23 that the perovskite materials with the flatter surface displays a strong enhancement of the polar instability, while those that are significantly buckled shows its suppression. In the bulk  $P4mm$  PZT the PbO atomic layer is more buckled than the BO $_2$  one. In the capacitor geometry the interfacial relaxation at the  $P^+$  interface enhances the rumpling of the former, while notably reduces that of the latter.

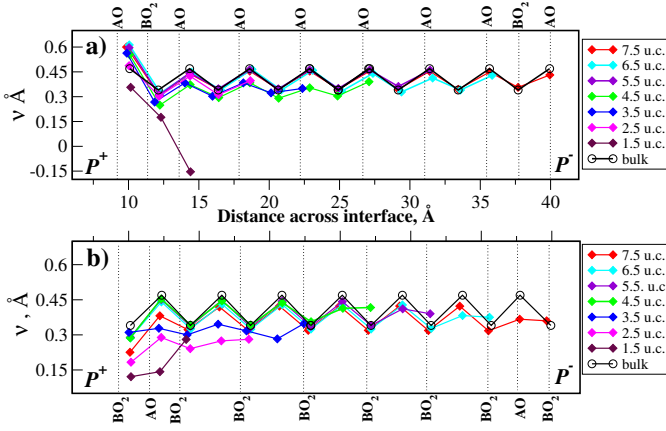


Figure 3. Dependence of the rumpling parameter,  $v$  with respect to the slab thickness and termination: a) Pt/PZT<sub>AO</sub> and b) Pt/PZT<sub>BO<sub>2</sub></sub> systems. Open black circles corresponds to bulk PZT, while coloured ones corresponds to PZT in capacitor geometry with different thickness from 1.5 to 7.5 unit cells.

### C. Switching

The interfacial reconstruction and bond formation may influence the switching characteristics of a capacitor because the process of switching requires a reversion of the polar state of ferroelectric, which leads to a swap between  $P^+$  and  $P^-$  sides of the capacitor. Relative stability of the ferroelectric (FE) state versus the paraelectric (PE) state may be affected by the interfacial reconstruction and important in understanding the switching properties of capacitors.

We have found that a PZT-based capacitor exhibits a higher PE state energy than that of the FE state for all studied terminations and thicknesses (See further details in the Supplementary Information). With  $n > 4.5$  u.c. the switching barrier of Pt/PZT<sub>AO</sub>/Pt converges to 0.41 eV per formula unit, while that for Pt/PZT<sub>BO<sub>2</sub></sub>/Pt gives a smaller value of 0.26 eV per formula unit. Both barriers are smaller than 0.451 eV barrier for bulk PZT. The switching barrier for bulk PZT is expectedly high because it has been calculated for an ideal material free of defects (domain walls, metal contacts, vacancies). Clearly, the presence of interfaces affects the switching barrier.

We suggest that the switching barrier for the Pt/PZT<sub>BO<sub>2</sub></sub>/Pt is smaller because the interfacial layer is affected by polarisation reversal in a small amount, i.e. there is no physical bond breaking at the interface, although bond lengths are modified. In addition, the Pt/PZT<sub>BO<sub>2</sub></sub>/Pt shows flatter atomic layers than Pt/PZT<sub>AO</sub>/Pt, thus less energy is required to revert the first system. In contrast, switching of Pt/PZT<sub>AO</sub>/Pt requires the transformation of the interfaces with a strong Pt-O bonding (the  $P^+$  side) to non-bonding ( $P^-$ ), which consists in bond breaking.

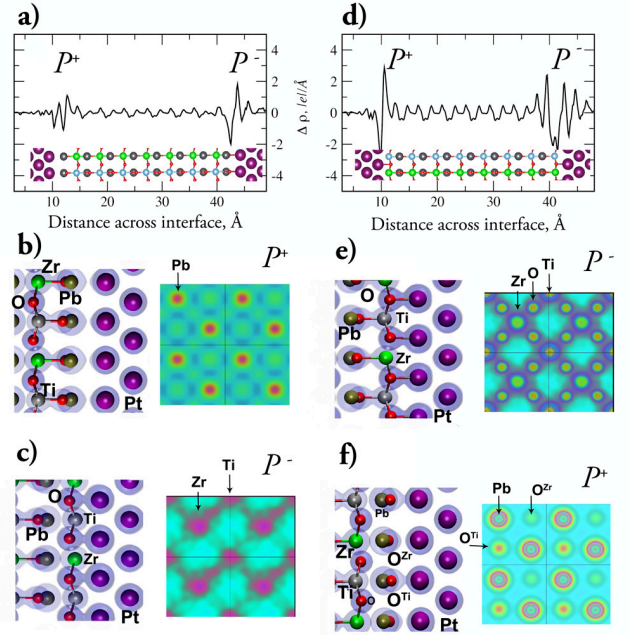


Figure 4. The planar average of charge density difference of the Pt/PZT<sub>(7.5)</sub> system and the sum of the isolated metal and perovskite densities for a) Pt/PZT<sub>AO</sub> and d) Pt/PZT<sub>BO<sub>2</sub></sub>. The projections of electron charge density on b) ( $xz$ ) and ( $xy$ ) projections for  $P^+$  interface of Pt/PZT<sub>AO</sub>.  $P^+$  exhibits a larger population of the density originated from  $O^{Ti}$ , while  $P^-$  shows homogeneous weak population. e) ( $xz$ ) and ( $xy$ ) charge density projections for the  $P^+$ , f) ( $xz$ ) and ( $xy$ ) projections for the  $P^-$  interface of Pt/PZT<sub>BO<sub>2</sub></sub>. The  $P^+$  interface shows the charge density localised at the interfacial bonds, while  $P^-$  exhibits a lesser density at the interface with an asymmetry associated with  $O^{Zr}$  species.

### D. Charge density distribution

The asymmetry of interfacial bonds related to the different chemical (in a sense of AO- and BO<sub>2</sub>-terminations), and the electrical environment (i.e. the presence of  $P^+$  and  $P^-$  interfaces), indicates a strong charge redistribution at Pt/PZT interfaces that would affect its electronic properties. Further, we provide an insight into the redistribution of the charge density,  $\rho$ , in the Pt/PZT/Pt capacitors. For this, we decompose the system into its perovskite and electrode components, and calculate charge densities separately in respective frozen capacitor geometry. The difference between the charge densities of the Pt/PZT/Pt capacitor, and the sum of isolated Pt and PZT systems, give the charge redistribution,  $\Delta\rho$ , caused by the interface (Fig. 4). The largest effect of the charge redistribution is at the interface itself. Inside the ferroelectric  $\Delta\rho$  exhibits regular oscillations of a small amplitude, indicating the long range effect of the density redistribution. Interesting, that the amplitude exhibited by the Pt/PZT<sub>BO<sub>2</sub></sub> is twice larger than the that in the Pt/PZT<sub>AO</sub>.

The analysis of the charge density at the crossover of  $P^-$  and  $P^+$  interfaces provides an insight into the charac-



ter of interfacial bonds (Fig. 4b, c, e, f). In particular, the Pt/PZT<sub>BO<sub>2</sub></sub> shows a dense homogeneous population of the charge density for both,  $P^+$  and  $P^-$ , interfaces. This corresponds to strong chemical interactions followed by the charge transfer between Pt and the outermost layer of PZT. Despite the repulsion between cations at the  $P^-$  interface, the oxygen states hybridise with Pt states.

In contrast, the Pt/PZT<sub>AO</sub> interface exhibits a weak population of the charge density at the  $P^-$  interface due to the repulsion between closely located positive charges of Pt and Pb cations. We note the  $P^+$  and  $P^-$  asymmetry in the hybridisation between Pt and O states. The  $O^{Ti}$  species exhibit charge density population at the Pt surface, while  $O^{Zr}$  shows the density localised in the ferroelectric.

To provide quantitative insight into the charge redistribution in a Pt/PZT<sub>7.5</sub>/Pt system we have performed the analysis of the Bader charges [24]. For the reference, the Bader charges of oxygen species in bulk PZT vary as  $-1.22 |e|$  for species in Pb-O-Pb bonds, and as  $-1.05 |e|$  and  $-1.28 |e|$  for  $O^{Ti}$  and  $O^{Zr}$ , respectively.

We found that interfacial Pt species show the charge modification of  $-0.3$  and  $+0.3 |e|$  in Pt/PZT<sub>AO</sub>/Pt, and  $-0.2$  and  $+0.2 |e|$  in Pt/PZT<sub>BO<sub>2</sub></sub>/Pt at the  $P^+$  and  $P^-$  interfaces, respectively.

At the  $P^+$  side of Pt/PZT<sub>AO</sub> interface the  $O^{Ti}$  species become  $0.07 |e|$  more electronegative in comparison to bulk, while the  $O^{Zr}$  loose  $0.08 |e|$ . However, at the  $P^-$  the charge variation is more pronounced of  $-0.39 |e|$  and  $+0.16 |e|$  for the  $O^{Ti}$  and  $O^{Zr}$ , respectively (See notations in Fig. 4).

The anions at the Pt/PZT<sub>BO<sub>2</sub></sub> interfaces become less electronegative (see Fig. 4) with charge reduction of  $0.11 |e|$  and  $0.2 |e|$  at the  $P^+$  and  $P^-$  interfaces, respectively. In addition, Zr cations at the Pt/PZT<sub>BO<sub>2</sub></sub> interface became  $0.02 |e|$  and  $0.06 |e|$  more electropositive in comparison to the bulk at the  $P^+$  and  $P^-$  sides, respectively. Meanwhile, Ti species show the largest modification of the charge: at the  $P^+$  interface Ti ion became  $0.5 |e|$  less electropositive, while at the  $P^-$  it gains  $0.154 |e|$ .

The described interfacial charge redistribution has a good correspondence with the projected charge density (Fig. 4b, c, e, f). The Bader charge analysis demonstrates that Pt/PZT/Pt capacitors are characterised by a strong redistribution of the charge, which leads to the formation of unequal local dipoles at the  $P^+$  and  $P^-$  interfaces, where the Pt/PZT<sub>AO</sub> interface shows effectively larger formed dipoles than that at the Pt/PZT<sub>BO<sub>2</sub></sub> interface.

### E. Electronic properties

For most practical applications, it is highly desirable for a capacitor to be insulating to  $dc$  current. An undesirable source of heating and power consumption is related to the transmission of electrons via non-zero conductivity or direct tunnelling.

To provide an insight into the electronic properties of metal/oxide interfaces we have constructed PDOS for Pt/PZT<sub>AO</sub>/Pt and Pt/PZT<sub>BO<sub>2</sub></sub>/Pt capacitors for the different PZT thicknesses. We found that thin systems, with  $n_c < 4.5$

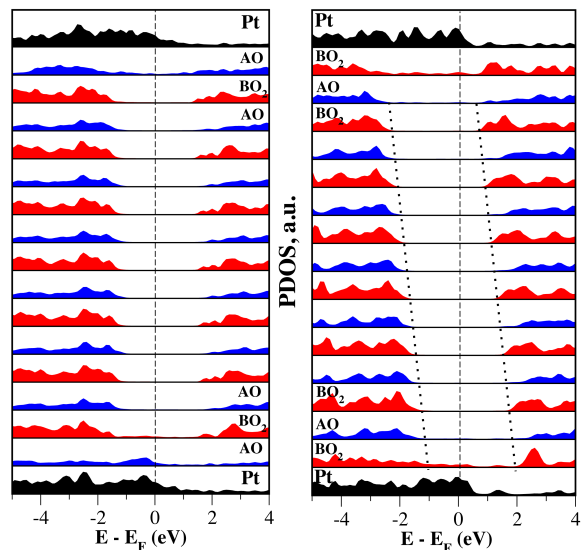


Figure 5. Projected Density of States for atomic layers of (a) Pt/PZT<sub>AO</sub>/Pt and (b) Pt/PZT<sub>BO<sub>2</sub></sub>/Pt capacitors with  $n=7.5$  u.c. Red, blue and black areas correspond to AO-, BO<sub>2</sub>-, and Pt atomic layers, respectively. The vertical broken line depicts the Fermi level, while dotted lines depict top of the valence band and the bottom of the condition band of the PZT film.

u.c., exhibit populated electronic states at the Fermi level in the central layer of the system (See Supplementary Information). The increase of  $n$  leads to an opening of the band gap, and its value converges to  $2.8$  eV corresponding to the band gap of the bulk PZT calculated with GGA level and expectedly underestimated in comparison to the experimental value.

In Fig. 5 the PDOS for Pt/PZT<sub>7.5</sub>/Pt with AO- and BO<sub>2</sub>- terminations of PZT are shown. One can see that the layers adjacent to the electrode interface exhibit states that cross the Fermi level, thus, the system is locally metallic. For the Pt/PZT<sub>AO</sub>/Pt capacitor in the middle of the PZT, the states at the Fermi level vanish, which implies that the system is locally insulating. The PDOS of the conduction and the valence bands converges quickly to the bulk curve when moving away from the interface.

Furthermore, the PDOS of each layer of Pt/PZT<sub>BO<sub>2</sub></sub>/Pt capacitor appears systematically shifted with respect to the neighbouring layers, which is consistent with the presence of the depolarising field. The increase of the PZT thickness leads to cross of the Fermi level with unoccupied levels of PZT. By extrapolating this straight line, we would see that it crosses the Fermi level at the thickness of  $n=9.5$  u.c.

### F. Screening properties

Imperfect screening leads to the appearance of a depolarising field that reduces the dielectric response and can destabilise the single-domain ferroelectric state. Thus, an insight into the interaction of ferroelectric and electrode materials is crucial for the device design. We further anal-

used the planar averaged potential to tackle the variation of this property across the Pt/PZT/Pt capacitor. We plot the macroscopic-average electrostatic potential (Eq. 5), in Fig. 6 for Pt/PZT<sub>AO</sub>/Pt and Pt/PZT<sub>BO<sub>2</sub></sub>/Pt capacitors together with the potential in the freestanding PZT slabs in frozen bulk geometry with a similar termination.

Due to the polarisation orientation, the  $P^+$  and  $P^-$  surfaces of the ferroelectric slab have different work functions causing the potential drop across the slab,  $\Delta_1$ , and the potential difference between two asymmetric vacuum potentials,  $\Delta_2$  (See Fig. 6). We found that the electronic screening properties of the PZT-based capacitors depend crucially on the local chemical environment. Indeed, the potential drop in the AO-terminated slab ( $\Delta_2 - \Delta_1 = 0.17$  V) is greater than that inside the Pt/PZT<sub>AO</sub>/Pt capacitor  $\Delta_3 = 0.015$  V. In the absence of electrodes, the depolarising field of  $6.1$  mV/Å would bring the freestanding slab into the paraelectric state, while in the capacitor geometry the field is cancelled mostly due to metallic screening from the electrodes that compensates the polarisation charge. Indeed, in Pt/PZT<sub>AO</sub>/Pt the residual depolarising field inside the film is as small as  $0.5$  mV/Å.

Similarly, for the BO<sub>2</sub>-terminated slab we found a potential drop  $\Delta_2 - \Delta_1$  of  $0.09$  V, while the potential drop inside the BO<sub>2</sub>-terminated capacitor is of  $0.14$  V much larger than that of the AO-terminated system (Fig. 6c, d). The residual depolarising electric field in the Pt/PZT<sub>BO<sub>2</sub></sub>/Pt capacitor is of  $4.5$  mV/Å, that produces a linearly increasing electrostatic potential on the film (Fig. 6b). The existence of such a depolarising field is caused by the imperfect screening at the interface [21, 25, 26], which is a property of the interface as a whole (that is, the metal, the ferroelectric and the specific interface geometry). We assume the origin of the depolarising field is due to strong chemical bonds formed at the Pt/PZT<sub>BO<sub>2</sub></sub> interfaces. We therefore emphasise the importance of the chemical environment leading to the inequivalent work functions determining the ferroelectric behaviour of ultrathin films at this range of thicknesses.

#### IV. SUMMARY

In this work we studied the structural and electronic properties of Pt/PZT interfaces with different, PbO- and TiZrO<sub>2</sub>- terminations in varied thickness capacitor geometry. We showed that the chemical environment at the interface plays a critical role in determining the interfacial bonds, promoting oxygen rotation and charge redistribution. Our findings reveals that the Pt/PZT<sub>BO<sub>2</sub></sub> interface is  $94.5$  meV/Å more energetically stable than Pt/PZT<sub>AO</sub> one. This is related to strong interfacial bonds formed at the Pt/PZT<sub>BO<sub>2</sub></sub> interfaces, while the Pt/PZT<sub>AO</sub> is characterised by weak interfacial bonds. We expect a suppressed polarisation in the Pt/PZT<sub>BO<sub>2</sub></sub>/Pt capacitors due to a flattening of its outermost atomic layers, while the

Pt/PZT<sub>AO</sub>/Pt capacitor shows an enhanced rumpling parameter at the  $P^-$  interface.

The ferroelectric state was found to be stable for all thicknesses of PZT films, although, thin capacitors with the thickness below  $4.5$  u.c. exhibit metal states in the gap.

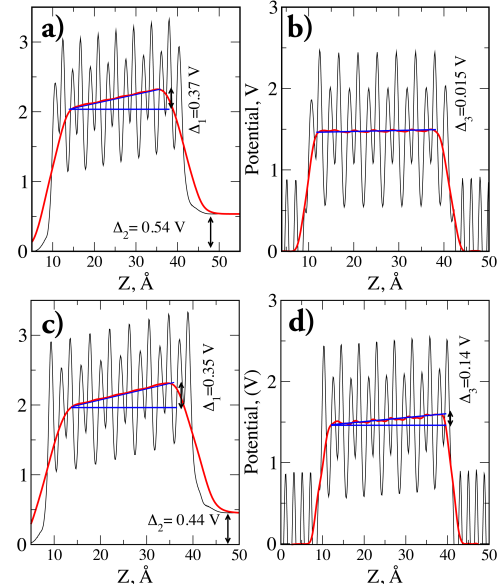


Figure 6. Planar averaged electrostatic potential in a) the frozen bulk geometry freestanding AO-terminated PZT slab exhibits the drop of potential  $\Delta_1 = 0.37$  V, difference between the two asymptotic vacuum potentials is  $\Delta_2 = 0.54$  V; b) freestanding BO<sub>2</sub>-terminated PZT slab with  $\Delta_1 = 0.35$  V, vacuum potential drop is  $\Delta_2 = 0.44$  V; c) AO-terminated PZT slab in capacitor geometry exhibits drop of potential of  $\Delta_3 = 0.14$  V; d) BO<sub>2</sub>-terminated PZT slab shows the drop of potential  $\Delta_3 = 0.090$  V.

The Pt/PZT interfaces are characterised by the strong charge redistribution leading to the formation of unequal local dipoles at the  $P^+$  and  $P^-$  interfaces, where the Pt/PZT<sub>AO</sub> interface shows an effectively larger dipole formed than that at the Pt/PZT<sub>BO<sub>2</sub></sub> interface. The Pt/PZT<sub>AO</sub>/Ptcapacitor exhibits a small depolarising field of  $0.5$  mV/Å, while the Pt/PZT<sub>BO<sub>2</sub></sub>/Ptcapacitor shows a depolarising field ten times larger. This is caused by the imperfect screening due to strong interfacial bonds formed at the Pt/PZT<sub>BO<sub>2</sub></sub> interfaces and suppressed rumpling of (ZrTiO)<sub>2</sub> outermost PZT layer.

We hope that our findings will provide a guidance to the synthesis of nanoscale capacitors, and allow for a better control of epitaxial growth of PZT films.

**Acknowledgements** AK is supported by the European Union's Horizon 2020 research and innovation programme under the Marie Skłodowska-Curie grant agreement No 796781. Author also acknowledges HPC-Europa programme for the access to ARCHER, Barcelona Supercomputing Centre.

[1] J. Scott, Annual Review of Materials Research **41**, 229 (2011).

[2] S. Zhang, X. Guo, Y. Tang, D. Ma, Y. Zhu, Y. Wang, S. Li,

- M. Han, D. Chen, J. Ma, B. Wu, and X. Ma, *ACS Nano* **12**(4), 3681 (2018).
- [3] C. Lichtensteiger, S. Fernandez-Pena, C. Weymann, P. Zubko, and J.-M. Triscone, *Nano Letters* **14** (8), 4205 (2014).
- [4] . A. K. Tagantsev and G. Gerra, *J. Appl. Phys.* **100**, 051607 (2006).
- [5] W. Al-Saidi and A. M. Rappe, *Physical Review B* , 155304.
- [6] F.-Y. Lin, A. Chernatynskiy, J. C. Nino, J. L. Jones, R. Hennig, and S. B. Sinnott, *J. Appl. Phys.* **120**, 045310 (2016).
- [7] A. Nozaka and Y. Masuda, *Ferroelectrics* **357**, 276 (2007).
- [8] F. Chen, R. Schafranek, W. Wu, and A. Klein, *J. Phys. D: Appl. Phys.* **44**, 155301 (2011).
- [9] I. Bucur, L. Tâase, L. Abramiuc, G.A.Lungu, C. Chirilă, N. Apostol, R.M.Costescu, R. Negrea, L. Pintilie, and C.M.Teodorescu, *Applied Surface Science* **432**, 27 (2017).
- [10] O. Auciello, J. F. Scott, and R. Ramesh, *Phys. Today* **51**, 22 (1998).
- [11] B. Noheda, D. E. Cox, G. Shirane, J. A. Gonzalo, L. E. Cross, and S.-E. Park, *Applied Physics Letters* **2059**, 6 (1999).
- [12] N. Zhang, H. Yokota, A. M. Glazer, Z. Ren, D. Keen, D. S. A. Keeble, P. A. Thomas, and Z.-G. Ye, *Nat. Commun.* **5**, 6231 (2014).
- [13] N. Setter, D. Damjanovic, L. Eng, G. Fox, S. Gevorgian, S. Hong, A. Kingon, H. Kohlstedt, N. Y. Park, G. B. Stephenson, I. Stolitchnov, A. K. Tagantsev, D. V. Taylor, T. Yamada, and S. Streiffer, *J. Appl. Phys.* **100**(5), 051606 (2006).
- [14] X. J. Lou, *J. Appl. Phys.* **105**, 024101 (2009).
- [15] A. K. Tagantsev, I. Stolichnov, E. L. Colla, and N. Setter, *J. Appl. Phys.* **90**, 1387 (2001).
- [16] H. Han, Y. J. Park, S. Baik, W. Lee, M. Alexe, D. Hesse, and U. Gosele, *Journal of Applied Physics* **108**, 044102 (2010).
- [17] S. J. Clark, M. D. Segall, C. J. Pickard, P. J. Hasnip, M. J. Probert, K. Refson, and M. C. Payne, *Zeitschrift fuer Kristallographie* **220**(5-6), 567 (2005).
- [18] D. Vanderbilt, *Phys. Rev. B* **41**, 7892 (1990).
- [19] Z. Wu and R. E. Cohen, *Phys. Rev. B* **73**, 135116 (2006).
- [20] A. Bogdanov, A. Mysovsky, C. J. Pickard, and A. V. Kimmel, *PCCP* **18**, 28316 (2016).
- [21] M. Stengel, P. Aguado-Puente, N. A. Spaldin, and J. Junquera, *Phys. Rev. B* **83**, 235112 (2011).
- [22] D. Pontes, L. Garcia, F. Pontes, A. Beltran, J. Andresa, and E. Longo, .
- [23] M. Stengel, D. Vanderbilt, and N. Spaldin, *Nature materials* **8**, 392 (2009).
- [24] W. Tang, E. Sanville, and G. Henkelman, *J. Phys.: Compute Mater.* **21**, 084204 (2009).
- [25] N. Sai, A. M. Kolpak, and A. M. Rappe, *Phys Rev B* **72**, 020101(R) (2005).
- [26] M. A. M. Polanco, I. Grinberg, A. M. Kolpak, A. V. Levchenko, C. Pynn, and A. M. Rappe, *Phys. Rev. B* **85**, 214107 (2012).